Earth and Planetary Science
https://journals.nasspublishing.com/index.php/eps

**ARTICLE**

# Magnetic Susceptibility Reveals Differential Retrogression in Meta-Mafic Enclave Consistent with Metamorphic *P–T* Estimation and Petrography

**Qiqi Ou[1,2], Ross N. Mitchell[1,2*], Lei Zhao[1*], Xiaofang He[3*], Rucheng Zhang[1,2]**

1. State Key Laboratory of Lithospheric Evolution, Institute of Geology and Geophysics, Chinese Academy of Sciences, Beijing, 100029, China
2. College of Earth and Planetary Sciences, University of Chinese Academy of Sciences, Beijing, 100049, China
3. School of Geoscience and Surveying Engineering, China University of Mining & Technology, Beijing, 100083, China

**Abstract:** Magnetic susceptibility is widely applied in geology, but its use in the study of metamorphic rocks has been limited due to the complex nature of metamorphism. In this study, analyzing a partially retrogressed mafic enclave within Archean TTG gneiss from the Jiaobei Terrane, North China craton, we incorporate magnetic susceptibility with conventional metamorphic (petrographic and major element) proxies in order to investigate profiles of metamorphic retrogression. The magnetic susceptibility results show more complete retrogression in the direction parallel to the tectonic fabric and partial retrogression perpendicular to it. This geophysical observation, which is broadly consistent with the petrological observations and *P–T* estimates, suggests that the availability of fluids and perhaps even non-lithostatic pressure play roles in the preservation of such differential retrogression. This study thus introduces magnetic susceptibility as a novel proxy in this context, revealing its utility in rapidly and quantitatively identifying variable retrogression gradients consistent with, but with more precision than, measured metamorphic pressures.

**Keywords**: Retrograde metamorphism; Retrogression; Magnetic susceptibility; Mafic enclave; Thermomagnetic susceptibility

*Corresponding Author:
Ross N. Mitchell, State Key Laboratory of Lithospheric Evolution, Institute of Geology and Geophysics, Chinese Academy of Sciences, Beijing, 100029, China; College of Earth and Planetary Sciences, University of Chinese Academy of Sciences, Beijing, 100049, China; *Email: ross.mitchell@mail.iggcas.ac.cn*
Lei Zhao, State Key Laboratory of Lithospheric Evolution, Institute of Geology and Geophysics, Chinese Academy of Sciences, Beijing, 100029, China; *Email: zhaolei@mail.iggcas.ac.cn*
Xiaofang He, School of Geoscience and Surveying Engineering, China University of Mining & Technology, Beijing, 100083, China; *Email: xiaofang.he@cumtb.edu.cn*

**Received:** 3 March 2024; **Received in revised form:** 19 April 2024; **Accepted:** 28 April 2024; **Published:** 30 April 2024

**Citation:** Ou, Q., Mitchell, R.N., Zhao, L., et al., 2024. Magnetic Susceptibility Reveals Differential Retrogression in Meta-Mafic Enclave Consistent with Metamorphic *P–T* Estimation and Petrography. *Earth and Planetary Science.* 3(1): 55–67. DOI: https://doi.org/10.36956/eps.v3i1.1048

DOI: https://doi.org/10.36956/eps.v3i1.1048

## 1. Introduction

Magnetic susceptibility, a commonly studied magnetic physical property, is highly valued by geologists due to its broad application and significant research implications. It is extensively applied in fields such as petrology, paleomagnetism, and ore geology, particularly in studies of sedimentary and igneous rocks [1]. In the study of metamorphic rocks, previous work has explored the relationship between the variations in rock magnetic parameters and metamorphic grade (or crustal depth), with Powell [2] first proposing a potential connection between these factors in 1970. Subsequently, some researchers have identified a clear relationship between susceptibility and metamorphic grade [3–5], while others have found no significant correlation between them [6–8]. This discrepancy can be attributed to several factors, including high temperatures and fluid activities partially or completely resetting magnetic minerals. But perhaps most critically, previous work did not always control for comparable lithologies at various metamorphic grades, thus potentially leading to spurious results as susceptibility can vary as much between various lithologies as different metamorphic grades. Circumventing this problem by controlling for lithology, Xu et al. [9] showed that eclogites reveal a notable link between magnetic susceptibility and retrograde metamorphism, indicating that higher degrees of retrogression correspond to increased magnetic susceptibility.

Based on these observations, this paper introduces the application of magnetic susceptibility to discuss its relationship with the degree of retrogression in amphibolite facies rocks. As can be seen from Figure 1, Fe-Ti oxides in mafic rocks exhibit predominantly pressure-dependent mineral stability fields, with increasing (approximate) pressure ranges: magnetite (< 8 kbar), ilmenite (~14 kbar), and rutile (> 11 kbar) (Figure 1A). Meanwhile, the magnetic susceptibilities of these minerals also range systematically, from high to low, where magnetite > ilmenite > rutile (Figure 1B). Through systematic sampling of a partially retrogressed mafic enclave in the Jiaobei Terrane of North China craton (Shandong Province) that combines measurements of magnetic susceptibility, thermomagnetic behavior, and petrological characteristics, this study effectively demonstrates the relationship between these factors. Moreover, it further explores the potential causes of these variations, enhancing our understanding of the geochemical processes influencing magnetic properties in metamorphic rocks.

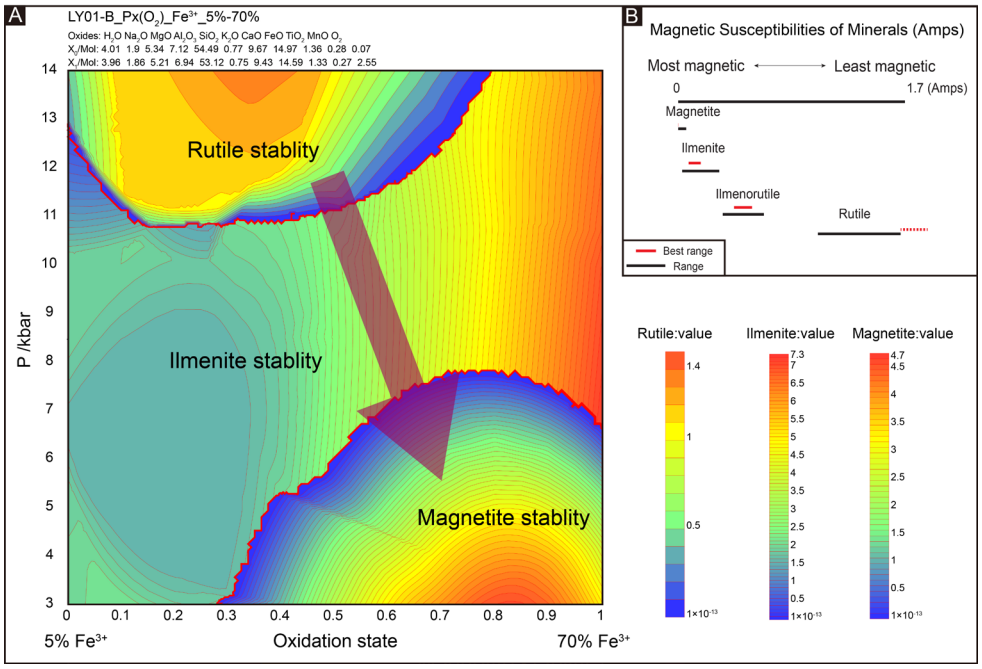


**Figure 1.** Metamorphic pressure–temperature (*P*–*T*) stability and magnetic susceptibility of ferromagnetic Fe-Ti oxides in a mafic amphibolite. (**A**) Phase diagram for Fe-Ti-oxides in a mafic protolith. Note the Fe-Ti-oxides are largely pressure dependent. (**B**) Relative magnetic susceptibilities (*k*) of Fe-Ti oxides relevant to metamorphosed mafic rocks.

Source: Modified from Rosenblum et al. [10].

## 2. Geological Setting and Sampling

The North China craton has a prolonged geological history that preserves important imprints of Earth history, including crust formation, stabilization, and tectonic events from the early Archean to the Cenozoic [11,13–17]. The North China craton can be divided into the Eastern and Western blocks separated by three Paleoproterozoic orogenic belts (from west to east): the Khondalite Belt, the Trans-North China Orogen, and the Jiao-Liao-Ji Belt (JLJB) (Figure 2A). Part of the JLJB, the Jiaobei Terrane on the eastern margin of the North China craton contains crucial insights into Precambrian tectonic evolution, marked by a rich record of Archean to Proterozoic geological events.

The Jiaobei Terrane is primarily composed of early Precambrian basement rocks intruded by Mesozoic granitoids. The early Precambrian rocks are further divided into Archean and Paleoproterozoic components. The Archean basement consists mainly of tonalite–trondhjemite–granodiorite (TTG) gneisses, granitoids, and associated plutonic rocks, with minor amounts of amphibolite and supracrustal rocks [18–20]. The Paleoproterozoic basement rocks are mainly composed of meta-sedimentary rocks and meta-magmatic intrusive bodies of the Jingshan Group and Fenzishan Group (Figure 2B). These Paleoproterozoic units unconformably overlay the Archean TTG gneisses [21]. The rocks of the Jingshan Group record a metamorphic transition from high-amphibolite facies to granulite facies, along with extensive anatexis, while those of the Fenzishan Group were metamorphosed from greenschist facies to low-amphibolite facies. In addition, mafic dikes and blocks have been found in Archean TTGs, and these mafic rocks are primarily of Archean protolith. Many of these Archean mafic rocks exhibit evidence of two stages of Neoarchean (ca. 2.5 Ga) and Paleoproterozoic (1.9–1.8 Ga) metamorphism [11,18,22–24].

The studied outcrop is located in the Qixia area of the Jiaobei Terrane, east North China craton (Figure 2). The studied outcrop comprises deformed mafic enclaves, which are garnet-bearing amphibolite and occur within the ca. 2.5 Ga TTG gneiss, with one enclave in particular being the focus of this detailed study (Figure 3). Both the garnet amphibolite and TTGs experienced Paleoproterozoic metamorphism (1.9–1.8 Ga) [24]. Aerial imagery of the outcrop reveals a tectonic fabric and shear sense that have led to the boudinage of the mafic enclaves, with its shear plane predominantly oriented approximately vertically relative to the outcrop surface (Figure 3). Three samples were collected along a profile perpendicular to the metamorphic fabric from this single mafic enclave (GPS WGS84 datum: 37°19'55.0" N and 120°59'15.2" E), with samples positioned accordingly within the enclave: LY01-B (the most retrogressed sample at the edge), LY01-D (intermediate sample), and LY01-E (the least retrogressed sample in the core).

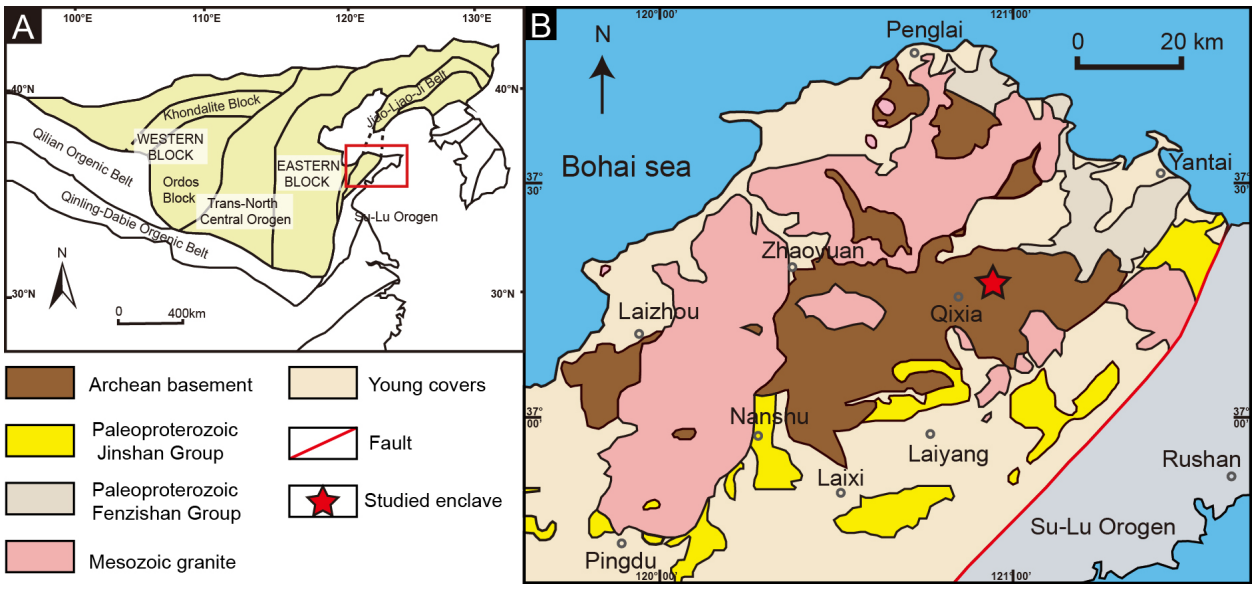


**Figure 2.** Geologic map of North China craton (**A**) and Jiaobei Terrane (**B**). Star indicates the location of the mafic enclave studied in detail in this study.

Source: Modified after Zhao et al. [11] and Zhang et al. [12].

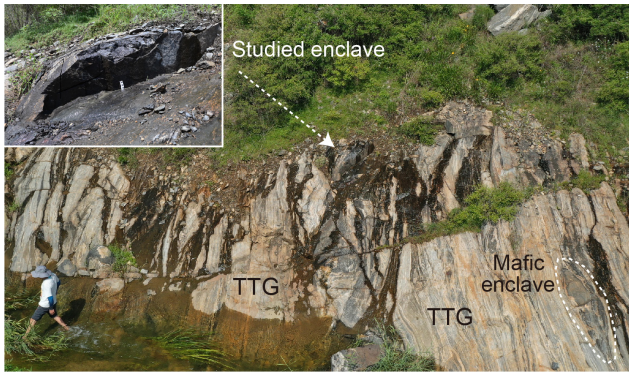


**Figure 3.** Garnet-bearing amphibolite enclaves in TTG at the studied outcrop. Aerial outcrop image (see geologist in bottom-left for scale) was taken with an unmanned aerial vehicle (UAV). The mafic enclave pictured in the zoomed-in inset picture was the focus of this detailed study (note 4 cm scale bar near the core of the enclave; see also Figure 4).

## 3. Methods

### 3.1 Petrography and Geochemistry

Outcrop photos were taken on multiple scales to characterize the studied rocks. Close-up photos were taken to make petrographic and metamorphic observations. Large-scale photos were taken with an unmanned aerial vehicle (UAV) for making structural deformation observations. Using a portable water-cooled diamond-bladed concrete saw, we sliced out a block sample spanning a vertical (fabric-perpendicular) profile of the studied mafic enclave. Thin sections were prepared from sub-samples of the block across the profile.

X-ray fluorescence (XRF) spectroscopy of major elements in whole-rock samples was measured at the Rock-Mineral Preparation and Analysis Laboratory at the Institute of Geology and Geophysics, Chinese Academy of Sciences (IGGCAS) using the PANalytical AXIOS Minerals instrument. This analysis utilized fused glass discs as the medium. The instrument, equipped with a Rh anode X-ray tube and 4 kW excitation power, is a sequential device featuring a single goniometer-based measuring channel covering the entire elemental measurement range from F to U. The concentration range extends from 1.0 ppm to % levels, and the analyses were conducted under vacuum conditions [25,26]. The specific data is presented in Table 1.

### 3.2 Magnetic Susceptibility and Thermomagnetic Behavior of Susceptibility

We measured magnetic susceptibility at the outcrop utilizing a standard-calibrated Terraplus KT-10R handheld magnetic susceptibility meter [27,28]. Measurements were made on flat surfaces where possible. Two profiles were measured, one oriented horizontally on the outcrop (being fabric-parallel) and one oriented vertically relative to the main outcrop surface (being fabric-perpendicular). As detailed in the section above, a block sample was also collected for a vertical profile in the fabric-perpendicular direction for further rock magnetic analysis back at the laboratory.

Using sub-samples of the collected block sample profile from the amphibolite enclave, thermomagnetic curves of susceptibility ($k$-$T$ curves) were obtained using the AGICO MFK2-FA KappaBridge instrument located at the "MagMin" laboratory at the Institute of Geology and Geophysics, Chinese Academy of Sciences (IGGCAS) in Beijing. Experiments were conducted using argon to prevent sample oxidation during heating and cooling. Thermomagnetic behavior of magnetic susceptibility aids in the identification of magnetic minerals and their domain states by revealing various behavioral features upon heating and cooling. The sharp loss of susceptibility upon heating to a certain temperature, for example, signifies the Curie point of a magnetic mineral. Impurities, e.g., Ti replacing Fe in magnetite, yield a temperature decrease of the Curie point. Curie point identification and thermal behavior below can then be coupled with thin-section analysis for fairly conclusive magnetic mineral identification, thus revealing which magnetic minerals are controlling the susceptibility trends measured on the outcrop.

**Table 1**. Major element (wt%) analyses of the samples from the Jiaobei Terrane, Shandong Province.

| Sample No. | $SiO_2$ | $TiO_2$ | $Al_2O_3$ | $TFe_2O_3$ | $Cr_2O_3$ | MnO | MgO | CaO | $Na_2O$ | $K_2O$ | ZnO | LOI | Total |
|---|---|---|---|---|---|---|---|---|---|---|---|---|---|
| LY01-B | 51.46 | 1.710 | 11.41 | 18.79 | 0.047 | 0.308 | 3.38 | 8.53 | 1.855 | 1.142 | 0.015 | 0.449 | 99.085 |
| LY01-D | 51.79 | 1.585 | 12.28 | 18.02 | 0.032 | 0.275 | 3.44 | 8.43 | 2.119 | 1.137 | 0.015 | 0.149 | 99.281 |
| LY01-E | 50.80 | 1.730 | 11.93 | 19.40 | 0.037 | 0.277 | 3.49 | 8.55 | 1.341 | 1.062 | 0.017 | 0.365 | 99.992 |

## 4. Results

### 4.1 Petrographic Observations

The studied mafic enclave is identified as garnet amphibolite, with field observations indicating that in the core region of the mafic enclave profile garnet grains are well-preserved, whereas in regions closer to the edge of the enclave the garnets have undergone noticeable retrogression (Figures 4 and 5). At the margin of the enclave (the most retrogressed sample LY01-B), the predominant minerals observed include hornblende (55–65 vol.%), garnet (10–15%), plagioclase, k-feldspar and quartz (20–30%), and minor amounts of magnetite, biotite and clinopyroxene. At the core of the enclave (the least retrogressed sample LY01-E), the primary mineral assemblage consists of hornblende (50–55 vol.%), garnet (20–25 vol.%), and plagioclase, k-feldspar and quartz (15–25 vol.%) along with minor occurrences of sphene and a relatively lower content of magnetite compared to the marginal portion. The garnet shows a decompression texture with amphibole and plagioclase coronas (Figure 5C). Both contain different amounts of opaque minerals, specifically 0.2–0.5% (at the edge) and 0–0.2% (in the core), mostly consisting of magnetite and ilmenite (Figure 5).

Overall, the modal proportion of garnet decreases from the core to the rim of the enclave, while the decompression texture of garnet becomes more prominent in the same direction. (Figures 4 and 5). In sample LY01-B at the enclave edge, most of the garnet has been replaced by plagioclase, hornblende, and magnetite, and plagioclase grains display relatively coarse sizes. There are two generations of hornblende, the prograde hornblende ($hornblende_1$) is coarse-grained and occurs in the matrix, while the retrograded hornblende ($hornblende_2$) occurs with the garnet symplectite. Accessory apatite is widely distributed in all samples. The retrograde reaction is $hornblende_1$ + garnet + $plagioclase_1$ = $plagioclase_2$ + $hornblende_2$ + magnetite.

### 4.2 Magnetic Susceptibility

Magnetic susceptibility measurements conducted in both profiles (Table 2; Figure 4C) indicate a consistently significant increase, spanning several orders of magnitude, from the core to the edge of the enclave. The measured $k$ depends on the intrinsic susceptibility ($k_i$), where $k = k_i/(1 + Nk_i)$, meaning that for high $k_i$ materials (such as magnetite) $k$ approaches $1/N$ (for 100% content). This allows an estimate of the magnetite content ($p$) in a sample by $k = p(1/N)$. The demagnetization factor ($N$) is 1/3 SI for a homogeneously magnetized sphere (SD), and increases from about 1/6 SI to 1/3 SI for low to high domain numbers of MD particles [29,30]. Accordingly, the vol% estimate ($p$×100) of magnetite for the sample with the highest $k$ value of

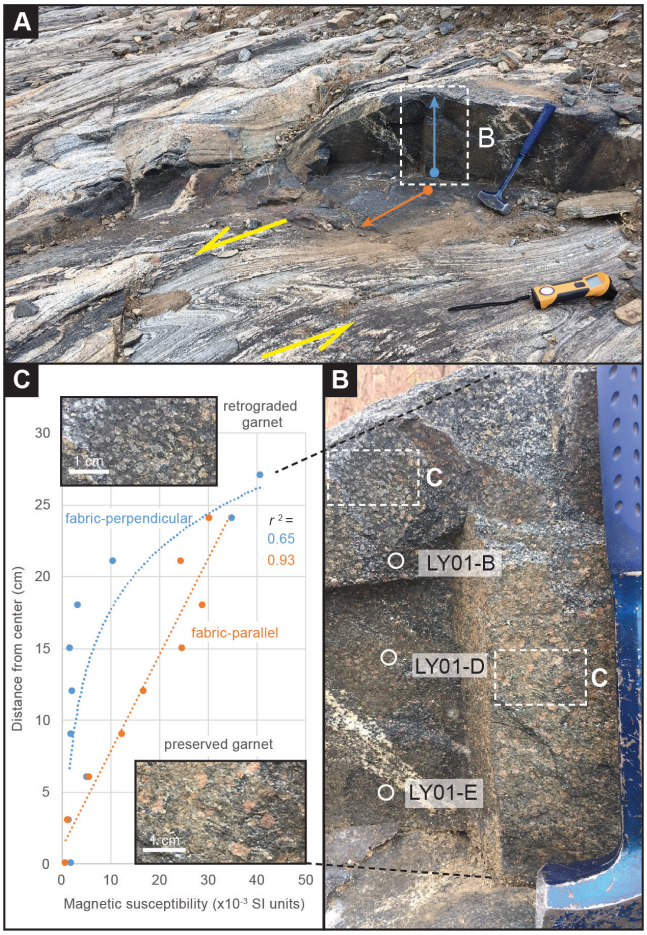


**Figure 4.** Directional differences in the magnetic susceptibility trends measured within the studied amphibolite enclave. (**A**) Two profiles were measured relative to the tectonic fabric (shear sense indicated by yellow arrows): one fabric-parallel profile measured on the horizontal face of the general outcrop (orange) and one fabric-perpendicular profile measured on the vertical face of the enclave (blue). (**B**) The fabric-perpendicular profile measured on the vertical face that was later cut with the concrete saw for a block sample of the entire profile. Note preserved garnet (red-colored) near the bottom of the image (enclave core) and retrogressed garnet (light-colored) near the top of the image (enclave edge). (**C**) Two susceptibility profiles measured fabric-parallel horizontally (orange curve) and fabric-perpendicular vertically (blue curve), including close-up inset images of the difference in garnet grain colors. The fabric-parallel data are fit with a linear regression and the fabric-perpendicular data are fit with an exponential function.

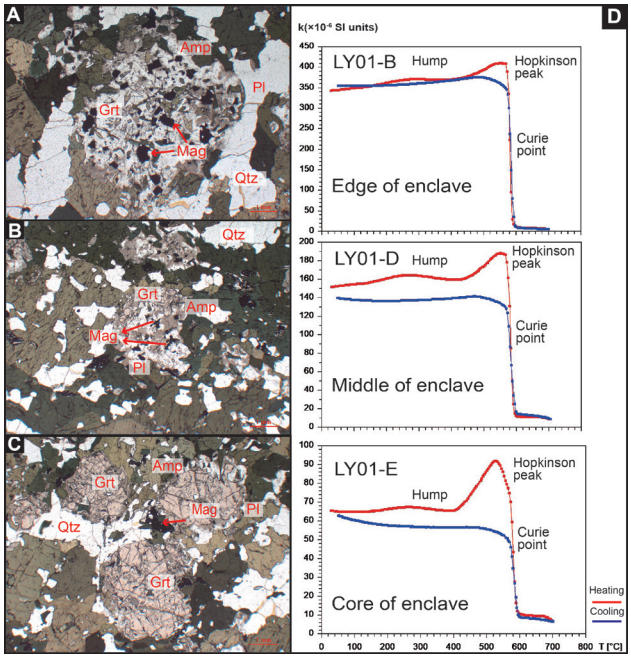


**Figure 5.** Mineralogy of amphibolite enclave profile from core (bottom) to edge (top) as determined with petrography and the thermomagnetic behavior of susceptibility. Samples LY01-B, LY01-D, and LY01-E are located at the edge, middle, and core of the enclave, respectively (Figure 4B). (**A**–**C**) Photomicrographs were taken in plane polarized light. Mineral abbreviations: Amp—amphibole, Pl—plagioclase, Grt—garnet, Mag—magnetite. (**D**) Thermomagnetic curves of susceptibility (*k*-*T*) of the same three samples.

0.04 SI in Table 2 would be approximately between 1% (SD) and 0.5% (MD). The susceptibility-based estimate of magnetite content, however crude, is broadly consistent with the aforementioned petrographic estimate of up to 0.5% magnetite at the enclave edge.

The notable rise in susceptibility from the core to the edge of the enclave coincides with indications of garnet retrogression observed in the petrography. Notably, however, the trends of susceptibility increase differ between the two profile orientations. Specifically, the fabric-parallel profile exhibits a linear increase, while the fabric-perpendicular profile demonstrates an exponential increase (Figure 4C). This divergence underscores a systematic difference in the distribution of susceptibility within the enclave.

## 4.3 Thermomagnetic Susceptibility Curves

First, the thermomagnetic curve of susceptibility (*k*-*T*) experiments (Figure 5D) supports the large increase in susceptibly from the core to the edge of the enclave as measured in the field (Figure 4C). The *k*-*T* curves furthermore allow for the determination, in concert with petrographic observations, of the magnetic mineralogy responsible for the large change in susceptibility across the enclave. Upon heating, all samples exhibit a small hump in the heating curves (peaking around 300 °C), which we interpret as very fine magnetite that reaches thermal relaxation (SD-SP transition, i.e., between single-domain and superparamagnetic behavior) at already intermediate temperatures [31].

Upon further heating, all three samples exhibit very clear and sharp Curie points (i.e., the temperature above which magnetic material becomes paramagnetic, where susceptibility drops sharply during heating) that are strikingly similar to each other and similar to the literature value for magnetite of 575–580 °C [32]. Such a high Curie point for the magnetite range observed in our samples is interpreted as pure "TM0" magnetite (i.e., with only Fe and zero Ti content). Finally, all three samples also exhibit notable but distinct Hopkinson peaks (i.e., an increase in susceptibility near the Curie point of magnetite), where the core of the enclave has much broader and higher Hopkinson peaks, the edge of the enclave has a more subdued Hopkinson peak, and that of the middle of the enclave exhibits intermediate behavior. According to the results of Dunlop et al. [33], a higher Hopkinson peak height indicates a smaller size of pseudo-single-domain (PSD) particles, which we would thus imply that the core of the enclave has small PSD magnetite particles whereas the edge would have comparatively larger PSD magnetite particles.

## 4.4 Phase Equilibria Modelling

We have conducted phase equilibria modelling on several of these samples. Phase equilibria calculations were performed using the software program Geo-PS 3.3.2 Section [34] with the internally consistent thermodynamic data set (ds633) of Holland and Powell [35]. The phase equilibrium modelling of sample LY01-E

**Table 2**. Magnetic susceptibility (× $10^{-3}$ SI units) data measured at the outcrop with the KT-10R meter along two profiles with different orientations within a deformed mafic enclave.

| Distance (cm) | 0 | 3 | 6 | 9 | 12 | 15 | 18 | 21 | 24 | 27 |
|---|---|---|---|---|---|---|---|---|---|---|
| Fabric-perpendicular | 2.14 | 1.66 | 5.39 | 2.21 | 2.36 | 2.03 | 3.51 | 10.7 | 35.2 | 40.9 |
| Fabric-parallel | 1.04 | 1.37 | 5.94 | 12.7 | 17 | 25 | 29.2 | 24.8 | 30.6 | |

Note: Distance is from core to edge of enclave. See Figure 4 for profile orientations.

shown in Figure 6 was conducted using the MnNCK-FMASHTO system. The *P–T* pseudo-section for the XRF effective bulk composition is presented in Figure 6. The simulated temperature range was 500–1,000 °C and the pressure range was 3–14 kbar. This figure reflects the stability ranges of the relevant minerals. As shown in Figure 6B, garnet is present across most of the *P–T* range, but its content gradually decreases as pressure decreases, corresponding petrographically to a gradual decomposition and reduction in garnet content with decreasing pressure. Clinopyroxene typically begins to appear around 700–750 °C and also appears at 500–600 °C under very high (> 11 kbar) or low pressures; thus, the presence of small amounts of clinopyroxene in the sample suggests that the metamorphic temperatures did not exceed 750 °C. Magnetite starts to appear at 650–700 °C, with the metamorphic pressure not exceeding 7 kbar (Figure 6B). Biotite content in the section is minor and is primarily influenced by temperature and does not appear significantly above ~760 °C (Figure 6C), suggesting that the metamorphic temperature did not exceed 760 °C. Amphibole isopleth phase diagrams (not shown) indicate that at 750 °C, amphibole content reaches 50%, consistent with petrographic observations described in Section 4.1. Both ilmenite and quartz are present from low temperatures and pressures to high temperatures and pressures.

Based on the petrographic features observed under the microscope, the stable mineral assemblage of the garnet-amphibolite during the peak metamorphic stage approximates Grt + Amp + Cpx + Kfs + Ilm + Qtz + melt, with very little clinopyroxene, which may have partially reacted due to the peak ultra-high temperature and pressure conditions and thus is not well preserved. Combined with the phase diagram, the temperature and pressure range for this stage is 740–760 °C and 9–11 kbar. The stable mineral assemblage during the retrograde metamorphic stage includes Grt + Amp + Bi + Pl + Cpx + Sph + Mag + Qtz + melt, with a temperature and pressure range of 700–740 °C and 3–5 kbar. This range of conditions is reflected in the *P–T* pseudosection (Figure 6A), where from core to rim of the enclave profile, the dominant factor driving retrograde metamorphism is pressure, representing a near-isothermal decompression (ITD) *P–T* path. Figure 6D shows the contents of each mineral assemblage at different times along the retrograde path, which is consistent with the described petrographic observations.

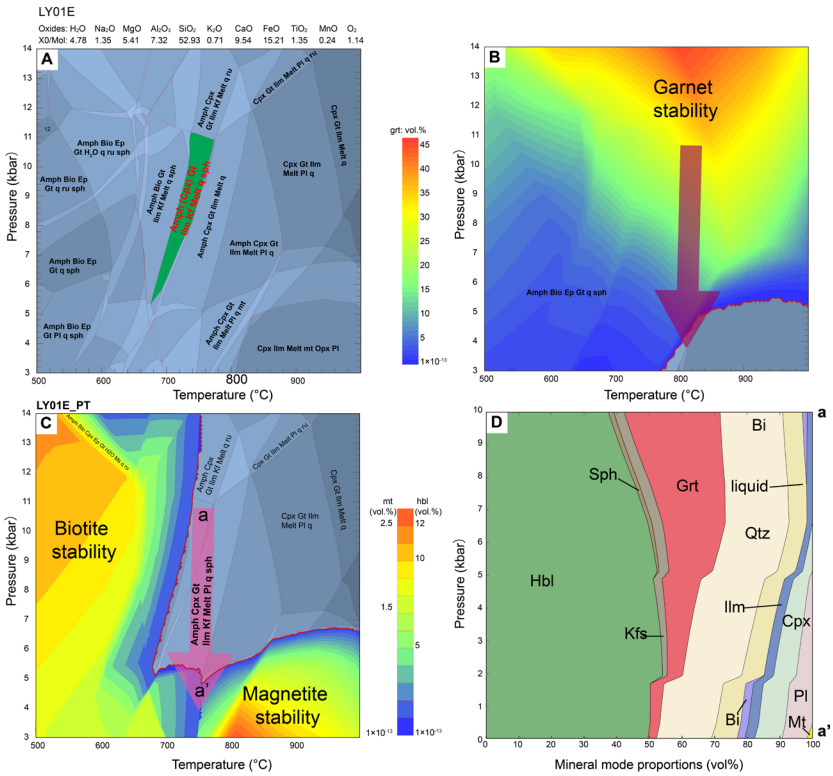


**Figure 6.** (**A**) *P–T* pseudo-sections calculated based on the XRF data for the least retrogressed sample (LY01-E) at the core of the enclave. (**B**) Isoline map of garnet, magnetite, and biotite in this system. (**C**) Isoline map of magnetite, and biotite in this system, and the near-isothermal decompression metamorphic path of this profile. (**D**) Mineral contents along the a-a' path.

## 5. Discussion

Using a multi-proxy geophysical and petrographic approach, our study of metamorphic rocks makes several discoveries about the relationship between retrogression and magnetic susceptibility. We show that susceptibility can be used to quickly—and even at the outcrop—identify quantitative trends in the degree of partial retrogression as preserved on small spatial scales such as a deformed mafic enclave. Although such gradients can be observed qualitatively with differences in mineralogy (e.g., garnet preservation vs. retrogression), susceptibility provides a quantitative proxy that can be measured readily and compared with petrographic-based metamorphic constraints. The previous work of Xu et al. [36] introduced the association of elevated susceptibility with retrograde phenomena in ultrahigh-pressure (UHP) eclogites. Our study thus goes one step further by demonstrating that magnetic susceptibility can also be used to detect differences in retrogression degree and that these differences are well correlated with rock properties and *P–T* estimation. Furthermore, we speculate on the possible causes of these differences.

We demonstrate with consistent lines of evidence from petrography and the thermomagnetic behavior of susceptibility that such gradients in susceptibility can be accounted for by different magnetic mineralogy related to garnet decomposition to other minerals (such as magnetite with high susceptibility) during retrogression (Figure 7). During retrograde metamorphism, the retrograde assemblage of plagioclase + hornblende$_2$ + magnetite was gradually formed by replacing garnet. During the more advanced retrograde metamorphic stage, the retrograded assemblage completely replaced the primary minerals in the studied sample. Therefore, the volume concentration of garnet decreases with increasing degrees of retrograde metamorphism. In contrast, with increased retrogression, the concentration of magnetite + hornblende will increase. Taking LY01-E as an example, the sample is situated in the core of the enclave with the least evidence of retrogression. The mineral assemblage indicates a gradual decrease in garnet (Figure 6B) content and concurrent appearance of minerals such as magnetite (Figure 6C), and biotite (Figure 6C).

Therefore, we interpret that large increase in susceptibility observed at the more heavily retrogressed edge of the enclave (Figure 4C) can be attributed to the formation of abundant pure magnetite (Figure 5) during retrograde metamorphism. Again, while increased magnetite content in the breakdown of garnet at the edge of the enclave can be observed petrographically (Figure 5A), the ~575–580 °C Curie point detected by thermomagnetic behavior of susceptibility can further identify pure TM0 (i.e., no titanium) magnetite (Figure 5D). This observation is consistent with magnetite being stable at lower *P* compared to ilmenite being stable at higher metamorphic pressures in mafic protoliths [9]. Although the mafic protolith of the studied mafic enclave likely started, before metamorphism,

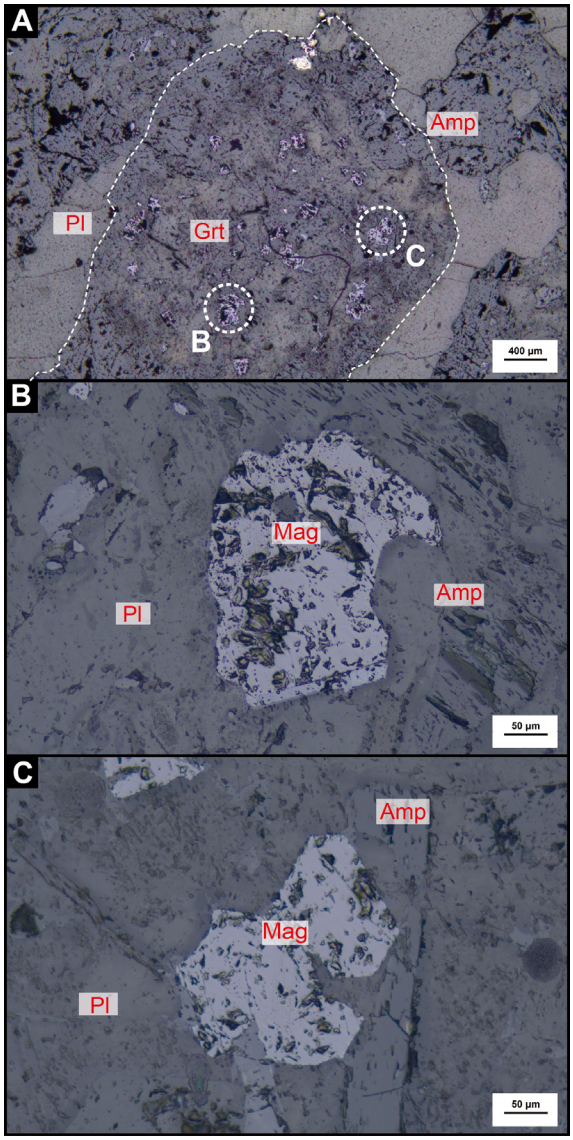


**Figure 7.** Photomicrograph taken under reflected light from the completely retrogressed sample from the edge of the mafic enclave (LY01-B). (**A**) The majority of garnet (Grt; grain boundary shown with dashed outline) has undergone retrogression and decomposition into plagioclase (Pl), hornblende, and magnetite (Mag). (**B–C**) Zoomed-in images of magnetite. Amp, amphibole.

with relatively abundant primary ilmenite and magnetite and therefore initially high susceptibility, prograde metamorphism would have destabilized relatively low-*P* magnetite, explaining why the better-preserved prograde core of the enclave has low susceptibility. Thus, to be clear, all the magnetite observed in this study is interpreted as secondary (metamorphic), not primary (magmatic).

The fact that retrogression is recorded at the edge of the enclave, and to a much lesser degree in the core, suggests that the presence/absence of fluids, respectively, controls the preservation of retrogression. The core was too dry to record the mineralogical changes that occurred during exhumation. The thermomagnetic behavior of susceptibility experiments further suggests, with the systematically different heights of Hopkinson peaks from core to edge of the enclave (Figure 5D), that the PSD particle size of the newly-formed magnetite during retrogression was very small near the core and larger near the edge of the enclave. More fluids circulating during retrogression at the edge of the enclave allowed for a lot of new magnetite (TM0) to grow and with larger PSD particles, whereas farther into the drier core of the enclave less new TM0 magnetite grew and with smaller PSD particle size. The elevated retrograde temperatures of ~550–800 °C documented from similar retrogressed mafic amphibolite in the region [12] would have further facilitated the enhanced growth of the large-particle magnetite at the edge of the enclave. Finally, fluids also likely influenced retrogression reaction rates, as well as mobilizing Fe and O for the formation of abundant high-susceptibility pure TM0 magnetite. This conclusion is consistent with the emphasis by Jamtveit et al. [37–39] on the significant influence of external fluids on retrograde metamorphism.

The mobility of fluids controlling the preservation of retrogression can also explain the contrasting trends in magnetic susceptibility for the profiles taken in different orientations of the enclave (parallel vs. perpendicular to the structural fabric), but an additional factor must also be invoked. All across the studied outcrop, many enclaves support the presence of fluid mobility related to the tectonic deformation, with enclaves exhibiting heterogeneity with fluid-rich and fluid-poor regions (Figure 8), consistent with the divergent susceptibility trends when measured along different orientations relative to the tectonic fabric. There are two possible explanations for the contrasting profiles. First, the lithologic heterogeneity of the surrounding TTG acquired during prograde deformation possibly allowed for more fluid mobility along fabric-parallel layering than across it (in the fabric-perpendicular direction). Second, non-lithostatic pressure may have additionally affected fluid mobility and controlled the extent of garnet transformation from edge to core in different directions. In the North American Cordillera, for instance, discrepancies between geobarometric pressures and palinspastic reconstructions based on field data suggest the prevalence of non-lithostatic pressure, which can have an impact on the calculation of the metamorphism temperature and pressure [40–42]. Neither explanation can be ruled out and they are also non-mutually exclusive. Further constraints would be needed to test their relative contributions.

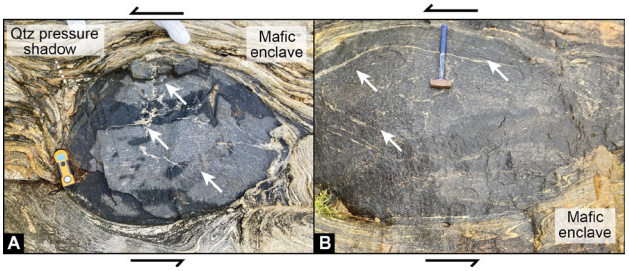


**Figure 8.** Evidence of fluid-related features in other mafic enclaves at the same outcrop. Arrows point to fluid-related melt channels. Note the heterogeneity of fluid-rich and fluid-poor regions. The quartz (Qtz) pressure shadow being an example of a low-pressure region. Shear sense is indicated. For scale, (**A**) 20-cm-long KT-10R magnetic susceptibility meter and (**B**) 30-cm-long rock hammer.

With the introduction of the utility of magnetic susceptibility for metamorphic field studies on a localized outcrop (e.g., < 1-m-scale in this study), the dynamics of differential retrogression preservation can be studied in new detail. The potential promise of magnetic susceptibility as a proxy for metamorphic pressure (Figure 1) is supported by a strong correlation between them in our study (Figure 9). Furthermore, whereas the typical pseudo-section approach to estimating pressure cannot distinguish (within uncertainty) between nearby samples along the profile of our study, susceptibility can successfully distinguish between them (Figure 9). Thus, given the proper mafic protolith, quick and easy variable retrogression gradients can be detected with susceptibility even *in situ* on the outcrop. Our contrasting profiles measured in different orientations with respect to the tectonic fabric further suggest that lithologic heterogeneity and/or non-lithostatic pressure play roles in controlling the mobility of fluids—lending a "third dimension" to

the study of partial retrogression, namely, differential retrogression preservation. Therefore, we suggest that magnetic susceptibility represents a previously under-utilized geophysical method in the study of metamorphic rocks. Investigating whether magnetic susceptibility can be used to directly calculate metamorphic pressure and be as useful for assessing prograde as well as retrograde metamorphism remains subjects for future research.

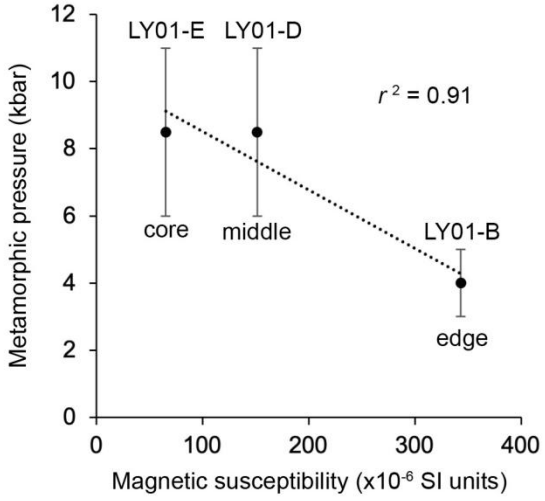


**Figure 9.** Inverse relationship between magnetic susceptibility and metamorphic pressure for the mafic protolith of this study (Table 3).

**Table 3**. Metamorphic pressure (kbar) and magnetic susceptibility (× $10^{-6}$ SI units; measured on the Kappa-Bridge) for three samples across the fabric-perpendicular (vertical) profile.

| Sample No. | LY01-B | LY01-D | LY01-E |
|---|---|---|---|
| Location | Near enclave margin | Middle of profile | Core of enclave |
| Metamorphic pressure | 3–5 | 6–11 | 6–11 |
| Magnetic susceptibility | 343.24 | 151.54 | 65.34 |

## 6. Conclusions

We find that a several-order-of-magnitude increase in magnetic susceptibility measured from the core to the edge of a partially retrogressed garnet amphibolite enclave is indicative of variable degrees of the transformation of garnet into high-susceptibility minerals like magnetite during retrogression, controlled by the availability of fluids, with the enclave margin being wet allowing for more complete retrogression and the core being dry and thus preserving only partial retrogression.

On the same mafic enclave, the core-to-edge trends of increasing magnetic susceptibility measured in different orientations relative to the tectonic fabric are found to be different (linear vs. exponential for fabric-parallel and fabric-perpendicular profiles, respectively), revealing either that lithologic heterogeneity acquired during prograde deformation and/or non-lithostatic pressure during retrograde stress affected fluid mobility and controlled the extent of garnet transformation from edge to core.

Our study introduces magnetic susceptibility as a novel, efficient proxy for quantitatively assessing the degree of partial retrogression in deformed mafic enclaves and demonstrates its effectiveness in detecting subtle variations in retrograde metamorphism influenced by fluid mobility, offering a less labor-intensive yet effective method for exploring the effects of fluid dynamics and potentially non-lithostatic pressure on metamorphism in field studies, thereby paving new avenues for future research within this domain.

## Author Contributions

The concepts and ideas in the paper were proposed and improved by Ross N. Mitchell, Lei Zhao and Xiaofang He; the petrology work was jointly completed by Qiqi Ou, Xiaofang He and Rucheng Zhang; the magnetic experiments were jointly completed by Qiqi Ou and Ross N. Mitchell; the writing and the first draft were completed by Qiqi Ou; Ross N. Mitchell, Lei Zhao, Xiaofang He and Rucheng Zhang provided revisions and suggestions.

## Funding

This research was funded by the Strategy Priority Research Program (Category B) of Chinese Academy of Sciences (XDB0710000) and the National Natural Science Foundation (grants 42372230 and 42220104008).

## Acknowledgments

Thanks to the anonymous reviewers as well as the editors for their constructive and insightful comments, which led to improvements in this study. Chun-Jing Wei from Peking University, and Ping-Hua Liu from Chinese Academy of Geological Sciences are thanked for their help during the field and very helpful discussions.

## Data Availability Statement

Magnetic susceptibility data measured on the outcrop in the field are presented in Table 2. Thermomag-

netic curves of susceptibility (*k*-*T*) data are available from the author upon reasonable request.

## Conflict of Interest

The authors declare that there is no conflict of interests regarding the publication of this article.

## References

[1] Tauxe, L., 2010. Essentials of paleomagnetism. University of California Press: Berkeley.
DOI: https://doi.org/10.1525/9780520946378

[2] Powell, D.W., 1970. Magnetised rocks within the Lewisian of Western Scotland and under the Southern Uplands. Scottish Journal of Geology. 6(4), 353–369.
DOI: https://doi.org/10.1144/sjg06040353

[3] Schlinger, C.M., 1985. Magnetization of lower crust and interpretation of regional magnetic anomalies: Example from Lofoten and Vesterålen, Norway. Journal of Geophysical Research: Solid Earth. 90(B13), 11484–11504.
DOI: https://doi.org/10.1029/JB090iB13p11484

[4] Schlinger, C.M., Khan, M.J., Wasilewski, P., 1989. Rock magnetism of the Kohistan island arc, Pakistan. Geological Bulletin, University of Peshawar. 22, 83–101.

[5] Krutikhovskaya, Z.A., Pashkevich, I.K., Simonenko, T.N., 1973. Magnetic anomalies of Precambrian Shields and some problems of their geological interpretation. Canadian Journal of Earth Sciences. 10(5), 629–636.
DOI: https://doi.org/10.1139/e73-063

[6] Wasilewski, P., Fountain, D.M., 1982. The Ivrea Zone as a model for the distribution of magnetization in the continental crust. Geophysical Research Letters. 9(4), 333–336.
DOI: https://doi.org/10.1029/GL009i004p00333

[7] Belluso, E., Biino, G., Lanza, R., 1990. New data on the rock magnetism in the Ivrea-Verbano zone (Northern Italy) and its relationships to the magnetic anomalies. Tectonophysics. 182(1–2), 79–89.
DOI: https://doi.org/10.1016/0040-1951(90)90343-7

[8] Williams, M.C., Shive, P.N., Fountain, D.M., et al., 1985. Magnetic properties of exposed deep crustal rocks from the Superior Province of Manitoba. Earth and Planetary Science Letters. 76(1–2), 176–184.
DOI: https://doi.org/10.1016/0012-821X(85)90157-8

[9] Liu, Q., Liu, Q., Zhang, Z., et al., 2007. Magnetic properties of ultrahigh-pressure eclogites controlled by retrograde metamorphism: a case study from the ZK703 drillhole in Donghai, eastern China. Physics of the Earth and Planetary Interiors. 160(3–4), 181–191.
DOI: https://doi.org/10.1016/j.pepi.2006.10.001

[10] Rosenblum, S., Brownfield, I.K., 2000. Magnetic suspectibilities of minerals. U.S. Geological Survey: Reston.
DOI: https://doi.org/10.3133/ofr99529

[11] Zhao, G., Sun, M., Wilde, S.A., et al., 2005. Late Archean to Paleoproterozoic evolution of the North China Craton: key issues revisited. Precambrian Research. 136(2), 177–202.
DOI: https://doi.org/10.1016/j.precamres.2004.10.002

[12] Zhang, R., Zhai, M., Zhao, L., 2022. Correlating metamorphic mineral assemblages with metamorphic ages in rocks recording multiple tectonothermal events: A case study of the Jiaobei terrane, eastern North China Craton. Precambrian Research. 377, 106731.
DOI: https://doi.org/10.1016/j.precamres.2022.106731

[13] Liu, D.Y., Nutman, A.P., Compston, W., et al., 1992. Remnants of ≥ 3800 Ma crust in the Chinese part of the Sino-Korean craton. Geology. 20(4), 339–342.
DOI: https://doi.org/10.1130/0091-7613(1992)020<0339:ROMCIT>2.3.CO;2

[14] Zhai, M., 2014. Multi-stage crustal growth and cratonization of the North China Craton. Geoscience Frontiers. 5(4), 457–469.
DOI: https://doi.org/10.1016/j.gsf.2014.01.003

[15] Zhai, M., Li, T.S., Peng, P., et al., 2010. Precambrian key tectonic events and evolution of the North China Craton. Geological Society, London, Special Publications. 338, 235–262.
DOI: https://doi.org/10.1144/SP338.12

[16] Zhai, M.G., Santosh, M., 2011. The early Precambrian odyssey of the North China Craton: A synoptic overview. Gondwana Research. 20(1), 6–25.
DOI: https://doi.org/10.1016/j.gr.2011.02.005

[17] Zhao, G., Cawood, P.A., 2012. Precambrian geology of China. Precambrian Research. 222–223, 13–54.
DOI: https://doi.org/10.1016/j.precamres.2012.09.017

[18] Tang, J., Zheng, Y.F., Wu, Y.B., et al., 2007. Geochronology and geochemistry of metamorphic rocks

in the Jiaobei terrane: Constraints on its tectonic affinity in the Sulu orogen. Precambrian Research. 152(1–2), 48–82.
DOI: https://doi.org/10.1016/j.precamres.2006.09.001

[19] Jahn, B.M., Liu, D., Wan, Y., et al., 2008. Archean crustal evolution of the Jiaodong Peninsula, China, as revealed by zircon SHRIMP geochronology, elemental and Nd-isotope geochemistry. American Journal of Science. 308(3), 232–269.
DOI: https://doi.org/10.2475/03.2008.03

[20] Wan, Y., Liu, S., Song, Z., et al., 2021. The complexities of Mesoarchean to late Paleoproterozoic magmatism and metamorphism in the Qixia area, eastern North China Craton: Geology, geochemistry and SHRIMP U-Pb zircon dating. American Journal of Science. 321(1–2), 1–82.
DOI: https://doi.org/10.2475/01.2021.01

[21] Zhu, G., Xu, J.W., 1994. The history of deformation and metamorphic evolution in the Jiaobei Area of Shandong Province. Journal of Hefei University of Technology (Natural Science). (3), 148–162. (in Chinese).

[22] Zhai, M., Guo, J., Liu, W., 2005. Neoarchean to Paleoproterozoic continental evolution and tectonic history of the North China Craton: A review. Journal of Asian Earth Sciences. 24(5), 547–561.
DOI: https://doi.org/10.1016/j.jseaes.2004.01.018

[23] Liu, J., Liu, F., Ding, Z., et al., 2013. The growth, reworking and metamorphism of early Precambrian crust in the Jiaobei terrane, the North China Craton: Constraints from U-Th-Pb and Lu-Hf isotopic systematics, and REE concentrations of zircon from Archean granitoid gneisses. Precambrian Research. 224, 287–303.
DOI: https://doi.org/10.1016/j.precamres.2012.10.003

[24] Zhao, L., Zou, Y., Liu, P., et al., 2023. An early Precambrian "orogenic belt" exhumed by the Phanerozoic tectonic events: A case study of the eastern North China Craton. Earth-Science Reviews. 241, 104416.
DOI: https://doi.org/10.1016/j.earscirev.2023.104416

[25] Xue, D.S., Su, B.X., Zhang, D.P., et al., 2020. Quantitative verification of 1:100 diluted fused glass beads for X-ray fluorescence analysis of geological specimens. Journal of Analytical Atomic Spectrometry. 35, 2826–2833.
DOI: https://doi.org/10.1039/D0JA00273A

[26] Zhang, D.P., Xue, D.S., Liu, Y.H., et al., 2020. Comparative study of three mixing methods in fusion technique for determining major and minor elements using wavelength dispersive X-ray fluorescence spectroscopy. Sensors. 20(18), 5325.
DOI: https://doi.org/10.3390/s20185325

[27] Mitchell, R.N., Kirscher, U., Kunzmann, M., et al., 2021. Gulf of Nuna: Astrochronologic correlation of a Mesoproterozoic oceanic euxinic event. Geology. 49(1), 25–29.
DOI: https://doi.org/10.1130/G47587.1

[28] Mitchell, R.N., Gernon, T.M., Cox, G.M., et al., 2021. Orbital forcing of ice sheets during snowball Earth. Nature Communications. 12, 4187.
DOI: https://doi.org/10.1038/s41467-021-24439-4

[29] Dunlop, D.J., 1983. On the demagnetizing energy and demagnetizing factor of a multidomain ferromagnetic cube. Geophysical Research Letters. 10(1), 79–82.
DOI: https://doi.org/10.1029/GL010i001p00079

[30] Dunlop, D.J., 1984. A method of determining demagnetizing factor from multidomain hysteresis. Journal of Geophysical Research: Solid Earth. 89(B1), 553–558.
DOI: https://doi.org/10.1029/JB089iB01p00553

[31] Zhang, Q., Appel, E., 2023. Reversible thermal hysteresis in heating-cooling cycles of magnetic susceptibility: A fine particle effect of magnetite. Geophysical Research Letters. 50(6), e2023GL102932.
DOI: https://doi.org/10.1029/2023GL102932

[32] Smith, D.O., 1956. Magnetization of a magnetite single crystal near the curie point. Physical Review. 102(4), 959–963.
DOI: https://doi.org/10.1103/PhysRev.102.959

[33] Dunlop, D.J., 2014. High-temperature susceptibility of magnetite: A new pseudo-single-domain effect. Geophysical Journal International. 199(2), 707–716.
DOI: https://doi.org/10.1093/gji/ggu247

[34] Xiang, H., Connolly, J.A., 2022. GeoPS: An interactive visual computing tool for thermodynamic modelling of phase equilibria. Journal of Metamorphic Geology. 40(2), 243–255.
DOI: https://doi.org/10.1111/jmg.12626

[35] Holland, T.J.B., Powell, R., 2011. An improved and extended internally consistent thermodynamic dataset for phases of petrological interest, involving a new equation of state for solids. Journal of metamorphic Geology. 29(3), 333–383.

DOI: https://doi.org/10.1111/j.1525-1314.2010.00923.x

[36] Xu, H., Jin, Z., Mason, R., et al., 2009. Magnetic susceptibility of ultrahigh pressure eclogite: The role of retrogression. Tectonophysics. 475(2), 279–290.
DOI: https://doi.org/10.1016/j.tecto.2009.03.020

[37] Jamtveit, B., Austrheim, H., Malthe-Sørenssen, A., 2000. Accelerated hydration of the Earth's deep crust induced by stress perturbations. Nature. 408, 75–78.
DOI: https://doi.org/10.1038/35040537

[38] Jamtveit, B., Malthe-Sørenssen, A., Kostenko, O., 2008. Reaction enhanced permeability during retrogressive metamorphism. Earth and Planetary Science Letters. 267(3–4), 620–627.
DOI: https://doi.org/10.1016/j.epsl.2007.12.016

[39] Jamtveit, B., Austrheim, H., 2010. Metamorphism: The role of fluids. Elements. 6(3), 153–158.
DOI: https://doi.org/10.2113/gselements.6.3.153

[40] Zuza, A.V., Levy, D.A., Mulligan, S.R., 2022. Geologic field evidence for non-lithostatic overpressure recorded in the North American Cordillera hinterland, northeast Nevada. Geoscience Frontiers. 13(2), 101099.
DOI: https://doi.org/10.1016/j.gsf.2020.10.006

[41] Gerya, T., 2015. Tectonic overpressure and underpressure in lithospheric tectonics and metamorphism. Journal of Metamorphic Geology. 33(8), 785–800.
DOI: https://doi.org/10.1111/jmg.12144

[42] Schmalholz, S.M., Podladchikov, Y.Y., 2013. Tectonic overpressure in weak crustal-scale shear zones and implications for the exhumation of high-pressure rocks. Geophysical Research Letters. 40(10), 1984–1988.
DOI: https://doi.org/10.1002/grl.50417